NUCLEAR SCIENCE AND ENGINEERING: **174**, 188–201 (2013)

Quasi-Differential Neutron Scattering in Zirconium from 0.5 to 20 MeV

D. P. Barry,* G. Leinweber, R. C. Block, and T. J. Donovan

Bechtel Marine Propulsion Corporation
P.O. Box 1072, Schenectady, New York 12301-1072

and

Y. Danon, F. J. Saglime, A. M. Daskalakis, M. J. Rapp, and R. M. Bahran

Rensselaer Polytechnic Institute, Department of Mechanical, Aerospace, and Nuclear Engineering
Troy, New York 12180-3590

Received January 10, 2012
Accepted August 10, 2012

Abstract—*High-energy-neutron-scattering experiments for elemental zirconium were performed at the electron linear accelerator facility at Rensselaer Polytechnic Institute. The scattering experiments were performed in the energy region from 0.5 to 20 MeV using the time-of-flight technique. The scattering system is composed of an array of eight EJ301 liquid scintillator detectors coupled to photomultiplier tubes. The detector array collects data simultaneously at various angles. The raw signals from each detector were digitized and transferred to a personal computer hard drive for storage. The digitized data were postprocessed, and pulse-shape analysis was performed to determine whether the pulse was the result of a gamma ray or a neutron being detected. The experimental results were compared with Monte Carlo transport calculations that simulated the experiment. This comparison was a way to benchmark several nuclear data libraries used in the Monte Carlo code. Ratios of the calculated data to the experimental data (C/E values) are presented and used to compare the nuclear data libraries. Results show that the experimentally observed scattering cross section is smaller than the one used in the evaluated libraries at energies between 10 and 20 MeV. For all energies and angles, the investigated nuclear data libraries agree with the experimental data to within 9%. Overall, the JEFF-3.1 and JENDL-4.0 libraries provide the best match to the experimental data.*

I. INTRODUCTION

Zirconium and zirconium alloys are important materials that are used by the nuclear industry in light and heavy water reactor systems. Zirconium alloys have favorable mechanical properties such as good strength, ductility, and resistance to water and steam corrosion under high-temperature and high-pressure conditions. Zirconium also has a relatively low thermal neutron absorption cross section, thereby decreasing parasitic reactions in the nuclear reactor core. Since zirconium finds use in reactor systems, it is desirable to know the cross section of zirconium as accurately as possible. This paper describes the measurement and benchmarking of the neutron scattering cross sections for zirconium.

The neutron differential scattering cross-section data play a substantial role in the behavior of nuclear reactor systems. For example, neutron differential scattering is part of the neutron transport equation, specifically the inscattering term $\Sigma_s(E' \rightarrow E, \Omega' \rightarrow \Omega)$ (Ref. 1). This term represents the contribution from neutrons scattering from energy E' and solid angle Ω' into E and Ω. The inscattering term becomes more complex at higher energies (above $\sim$1 MeV) as the scattering angular distributions become anisotropic and dependent on the neutron scattering angle. Neutron differential scattering data are

*E-mail: barryd3@rpi.edu

available from various evaluated nuclear data libraries, such as ENDF (Ref. 2), JEFF (Ref. 3), and JENDL (Ref. 4). The evaluated nuclear data in these libraries do not always agree with each other across the energy range of interest in nuclear reactor analysis.

To help determine whether the nuclear data libraries agree with experiment, the researchers at the Gaerttner Linear Accelerator Laboratory at Rensselaer Polytechnic Institute (RPI) developed a quasi-differential neutron scattering measurement. The term "quasi differential" signifies that the measurements are from neutrons that may have been scattered numerous times in the sample. An ideal double-differential neutron scattering experiment uses very thin samples and detectors that subtend a small solid angle. This ensures that only single-scattering events are detected at a precisely known angle. An example of such an experiment was performed for elemental zirconium by Smith and Guenther.[5] A quasi-differential measurement uses thick samples in which multiple scattering occurs. The increased signal strength reduces the experimental error and improves the benchmarking of neutron differential scattering cross-section data from the various nuclear data libraries. Benchmarking is accomplished by directly comparing the experimental data taken with the scattering detector system with MCNP simulations of the experiment.[6]

II. EXPERIMENTAL CONDITIONS

The RPI electron linear accelerator (LINAC) is used to generate a high-energy-pulsed-neutron source. Electrons are accelerated (to energy ~50 MeV) and collided with a neutron production target. The neutron production target[7] is composed of tantalum sheets in which the incident electrons rapidly lose energy via coulombic interactions and generate bremsstrahlung radiation. This bremsstrahlung radiation then interacts with the tantalum sheets to produce neutrons through the photonuclear process. The target is water cooled to dissipate the heat generated from the energy deposited in the tantalum sheets. The resulting neutron spectrum can be approximated as a sum of several evaporation spectra, which results in an overall spectrum with an effective temperature of ~0.5 MeV (Refs. 8 and 9). The data were taken using the time-of-flight (TOF) method.

Eight fast-neutron detectors were fabricated by ELJEN Technologies. Each detector is composed of a 12.7-cm (5-in.)-diam and 7.62-cm (3-in.)-long EJ301 proton recoil scintillator that is coupled to a 12.7-cm (5-in.)-diam Photonis XP4572/B photomultiplier tube (PMT). An array of eight detectors was used to simultaneously collect scattered neutrons at various angles. The detector array surrounded the sample at angles of 26, 52, 72, 90, 108, 120, 140, and 154 deg, each within an error of ±2 deg. These scattering angles were chosen so that the detectors were equally spaced in the direction cosine. The detectors were also placed around the sample to maximize the distance between each detector and, thereby, to minimize cross talk from detector-detector scattering. Each detector was placed at a distance of 50 ± 2 cm from the sample center of mass. The detectors were rigidly held in position through the use of 3.81-cm (1.5-in.)-diam aluminum rods attached to a 152 × 152 cm (5 × 5 ft) optical table. An example of such a detector arrangement is illustrated in Fig. 1. The scattering sample was held in place with a low-mass aluminum sample holder.

Agilent-Acquiris AP240 digitizers collected the raw signals from each of the eight detectors. The model AP240 is a dual-channel peripheral component interconnect (PCI) analyzer with 8-bit pulse-height resolution (256 levels) and an input bandwidth of 1 GHz (into 50 Ω). The AP240 is equipped with an onboard field-programmable gate array (FPGA), which performs analog-to-digital conversion at a sampling rate of up to 1 GHz in dual-channel mode and transfers the data to a host personal computer (PC) hard drive for storage and analysis. It should be noted that the FPGA will only transfer detector pulse-height data that exceed a predefined discriminator threshold. The data are transferred over the high-speed PCI bus

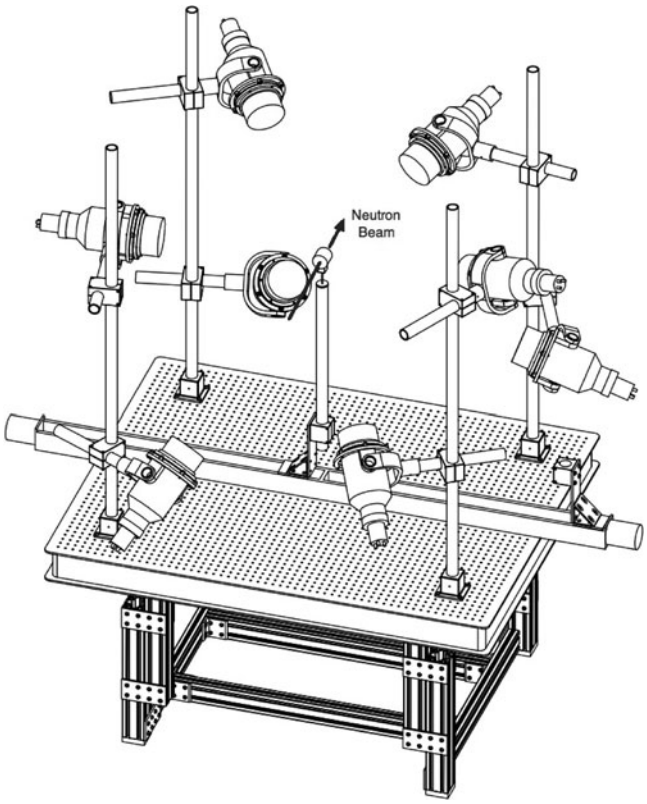

Fig. 1. Detailed view of the scattering experiment detector array. Detectors are secured in the proper positions through 3.81-cm (1.5-in.)-diam aluminum rods attached to a 152 × 152 cm (5 × 5 ft) optical table. The center of the sample is 75.9 cm (29.9 in.) above the tabletop.

at speeds up to 100 MBytes/s while the next data sequence is simultaneously collected. The anode signals from each detector PMT are connected directly to the input channels of the AP240 digitizer. A total of four digitizer boards were used in the system, each with two input channels. All of the digitizer boards were triggered by the same signal to ensure that all data were synchronized and collected simultaneously.

A data collection PC was used to control the experiment and stream the resulting scattering data to a hard disk. To increase data transfer speed and decrease file sizes, FPGA software was developed that selected and transmitted data only in the vicinity of the detector pulse. The software transfers the first 120 ns of data in each detector pulse at a sampling frequency of 1 GHz. The time interval of 120 ns was selected because it reflects the pulse duration of the EJ301 liquid scintillator response time. This sampling duration of 120 ns for each detector pulse sets the dead time of the scattering system. Previous studies have shown that the scattering system is capable of handling approximately 128 000 detector pulses per second[8,9] (pps). This counting rate limit is set by the data transfer rate from the board to the host PC.

A National Instruments NI6602 PCI board was used as a scaler for the beam monitor detectors. The NI6602 was triggered by a signal from the AP240 digitizer board, and the counter scalers were gated in time corresponding to an energy region from ~0.1 to ~280 eV. Two moderated fission chambers housed at a flight path of ~9 m away from the production target were used to monitor the neutron beam intensity. These beam monitors were used to normalize the background to the same neutron intensity as the data.

The PMTs were powered with negative high voltage from a CAEN unit (model 1733N) housed inside a SYS3527 chassis. Gain matching was performed with a ^{22}Na source by adjusting the high voltage of each PMT so that the digitized spectra were aligned at the Compton edge resulting from the 0.511-MeV annihilation gammas. This alignment was verified periodically during the experiment.

The detector efficiency and the flux incident on the sample were determined in previous work.[8,9]

The neutron beam was collimated into a 7.62-cm (3-in.)-diam beam at the sample location. A 2.54-cm (1-in.)-thick slab of depleted uranium (^{238}U) was used as a beam filter to attenuate unwanted gamma rays from the neutron production target (i.e., gamma flash). Depleted uranium was chosen instead of lead since depleted uranium has a relatively smooth neutron cross section in the energy region of interest. Therefore, the depleted uranium filter does not introduce significant structure into the neutron spectra measurements, and since the ^{238}U total cross section has been extensively evaluated,[2] it can be taken into account in the MCNP simulation of the experiment.

During the experiment, the LINAC was operated with a repetition rate of 400 pps, a 6-ns electron burst width, and an average current on target of 6 μA. Figure 2 shows an overview of the experimental setup.

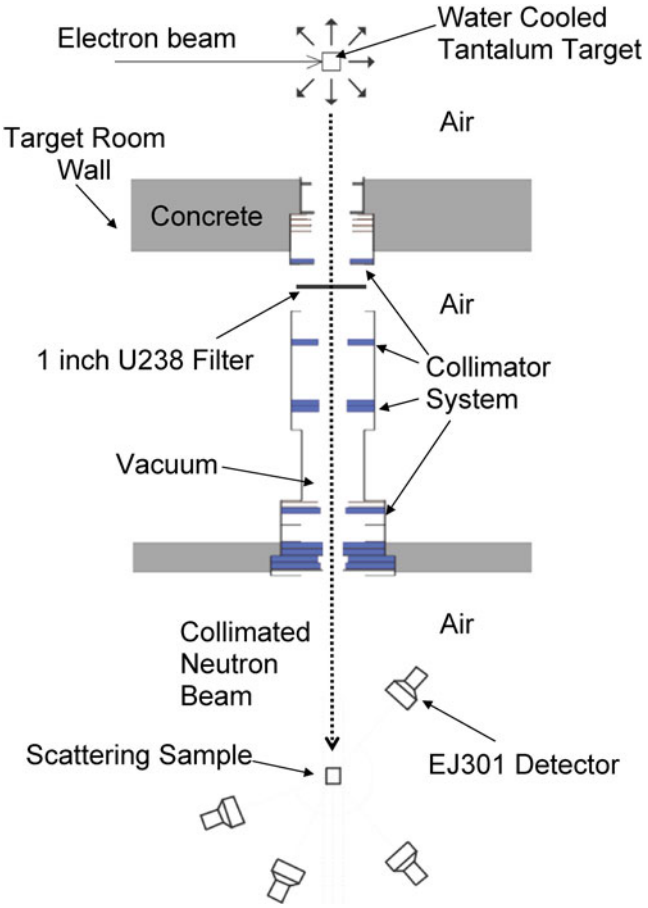

Fig. 2. Overview of the quasi-differential scattering experimental setup. Note: The drawing is not to scale, and only four of the eight detectors are shown.

A 7.5-cm-diam × 7-cm-thick cylinder of high-purity graphite was used as a reference to verify that the experiment was performed properly. Two different zirconium samples were used in the experiments, having thicknesses of 6 and 10 cm. Both zirconium samples had a 7.6-cm diameter. The properties of these samples are found in Table I. The samples were placed in the center of the incident neutron beam at a distance of 30.07 ± 0.02 m from the LINAC neutron production target. Each sample was oriented such that the cylindrical axis was parallel to the incident neutron beam.

A computer-controlled motorized sample changer was used to continuously cycle two mounted samples in and out of the beam (only one sample is shown in Fig. 1). The first sample was always the graphite sample that was centered in the beam for a specified amount of time and used as a reference. The second sample was zirconium, which was also centered in the beam with data collected for a longer amount of time. The background

TABLE I

Sample Dimensions and Number Density

Sample	Thickness (cm)	Diameter (cm)	Mass (g)	Number Density (atoms/b)
Carbon	7.005 ± 0.001	7.499 ± 0.003	521.87 ± 0.01	0.5925 ± 0.0002
Zirconium	6.007 ± 0.001	7.619 ± 0.003	1783.4 ± 0.1	0.2581 ± 0.0001
Zirconium	10.002 ± 0.001	7.621 ± 0.003	2967.2 ± 0.1	0.4296 ± 0.0001

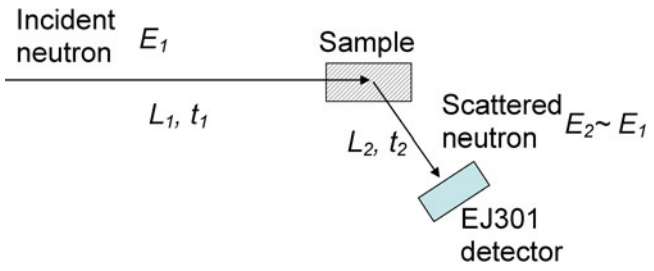

Fig. 3. An example of a possible flight path a scattered neutron will travel during the experiment.

was measured with neither sample in the beam while the LINAC was operating.

The TOF was found by measuring the total time it took for a neutron to travel from the production target to its subsequent detection after it was scattered by the sample. There are two flight paths involved in this process as illustrated in Fig. 3. The first flight path, L_1, is the distance from the production target to the sample, and it takes time t_1 for a neutron of energy E_1 to travel this distance. The second flight path, L_2, is the distance the scattered neutron with energy E_2 travels, in a time t_2, to the detector. The TOF t is mathematically expressed with the following relativistic formula:

$$t(E) = t_1(E_1) + t_2(E_2)$$

$$= \left(\frac{L_1}{c}\right) \frac{1}{\sqrt{1 - \left(\frac{m_n c^2}{E_1 + m_n c^2}\right)^2}}$$

$$+ \left(\frac{L_2}{c}\right) \frac{1}{\sqrt{1 - \left(\frac{m_n c^2}{E_2 + m_n c^2}\right)^2}} \quad , \qquad (1)$$

where m_n is the rest mass of the neutron and c is the speed of light in vacuum. The above TOF equation can be approximated by

$$t(E) \approx \left(\frac{\bar{L}}{c}\right) \frac{1}{\sqrt{1 - \left(\frac{m_n c^2}{E + m_n c^2}\right)^2}} \quad , \qquad (2)$$

where $\bar{L} = L_1 + L_2$ is the flight path distance of the scattered neutron. Because $L_2 \ll L_1$ and $E_1 \approx E_2 \approx E$, the flight time t is dominated by the incident neutron since $t_1 \gg t_2$. The flight path L_1 is measured to be 30.07 ± 0.02 m and represents the nominal distance from the production target to the sample center of mass. The flight path L_2 is 0.5 ± 0.02 m and represents the nominal distance from the sample center of mass to the front face of the detector. The effective flight path distance of the scattered neutron, $\bar{L}$, is 30.57 ± 0.03 m. This effective flight path was used for converting both the experimental data and the MNCP calculations from TOF to energy. The TOF t is measured in the experiment, and the energy of the incident neutron is approximated by

$$E(t) \approx m_n c^2 \left(\frac{1}{\sqrt{1 - \left(\frac{\bar{L}}{ct}\right)^2}} - 1 \right) \quad . \qquad (3)$$

This is the energy reported in this paper in order to compare various scattering spectra. The approximation does not degrade the comparison between the experimental results and the MCNP calculations since both employ the same mathematical transformation from TOF to energy.

III. DATA REDUCTION

A combination of X-rays, gamma rays, and neutrons are detected by the scattering system after the gamma flash. The gamma rays and X-rays are unwanted background arising from inelastic scattering of the neutrons and room background. Since we are only concerned with neutrons, pulse-shape analysis (PSA) was performed on each detector pulse to determine if the event was a result of a gamma ray or a neutron being detected. A least-squares approach was used to fit each detector pulse and

determine the ratio of the pulse's slow and fast components.[8,10] The slow-to-fast-component ratio allows the determination of whether the detected particle was a gamma ray or a neutron. Postprocessing software utilizing the ROOT data analysis framework[11] was used for the data analysis. The details of this software can be found in previous work.[8]

After the data were processed and PSA was performed, the counts per channel, D, was calculated as follows:

$$D = D_S - \frac{M_S}{M_O} D_O \ , \tag{4}$$

where

D_S = counts per channel for the sample-in condition

D_O = counts per channel for the sample-out condition

M_S = total monitor counts for the sample-in condition

M_O = total monitor counts for the sample-out condition.

Since the sample-in data were collected for a longer period of time than the sample-out data, the ratio of monitor counts, M_S/M_O, was used to normalize the sample-out data to perform the background subtraction.

Using the standard error propagation formula[12] in conjunction with Eq. (4), and noting that the error in the counts is the square root of the counts (e.g., $\Delta D_S = \sqrt{D_S}$), the statistical error in the counts per channel, ΔD, is found to be

$$\Delta D = \pm \sqrt{D_S + \left(\frac{M_S}{M_O}\right)^2 D_O + \left(\frac{M_S}{M_O^2}\right) D_O^2 + \left(\frac{M_S^2}{M_O^3}\right) D_O^2} \ . \tag{5}$$

IV. MCNP CALCULATIONS

Simulations of each experiment were performed using MCNP 5 (Ref. 6). The characteristics of the scattering experiment were modeled as accurately as possible, paying particular attention to the geometry, incident neutron flux energy distribution, and detector efficiency. The specific details of the MCNP model can be found in the work of Saglime.[8] The MCNP calculations resulted in a TOF spectrum for each evaluated neutron cross-section library, detector angle, and sample thickness. Each MCNP-calculated spectrum was normalized and compared with the experimental measurements performed at each angle. Since carbon was used as a reference, the normalizations were found by matching the areas under the spectra between experimentally measured carbon and the MCNP-calculated carbon, for each detector and angle in the energy region between 0.5 and 4 MeV. This energy region was selected because it had the best agreement between the shapes of the experimental and calculated spectra.

As discussed in Sec. VI, there are some disagreements between the experimental data and the MCNP calculation between 4 and ~9 MeV. Each detector had a slightly different efficiency and required a separate normalization. This normalization was then applied to the calculated zirconium MCNP spectra for the same detectors and angles. The zirconium MCNP calculations were repeated for four different libraries: ENDF-7.0, ENDF-6.8, JEFF-3.1, and JENDL-4.0. The MCNP calculations were performed using the appropriate combination of isotopic zirconium cross sections contained in each nuclear data library.

V. COMPARISONS

It is possible to visually compare differences between experimental data and MCNP calculations if there are large discrepancies between the two. Visual comparison has several shortcomings, such as the inability to see small differences and the lack of statistical error on the difference. Therefore, a more quantitative method was developed to determine the calculated-to-experimental ratio, or C/E value, in various energy groups. Six energy groups were selected to provide a way to compare data sets as a function of energy and are shown in Table II. The energy range for each group was chosen to achieve reasonable statistics. This method preserves the average value of the C/E in each group but does not take into account shape variations within the group. Additionally, Table II shows the shorthand notation describing each energy group that is used in subsequent figures.

For a given scattering angle Ω, sample thickness j, and energy group g, the C/E value is calculated by

TABLE II

Energy Groups Used in the Calculated-to-Experimental (C/E) Data Comparisons

Group Number	Energy Range (MeV)	Shorthand Notation
1	$0.5 \le E < 1.0$	[0.5,1)
2	$1.0 \le E < 2.0$	[1,2)
3	$2.0 \le E < 3.0$	[2,3)
4	$3.0 \le E < 4.0$	[3,4)
5	$4.0 \le E < 10.0$	[4,10)
6	$10.0 \le E \le 20.0$	[10,20]

summing all data points in the specified energy group and taking the ratio of the MCNP calculation to the experimental value, as follows:

$$(C/E)_{g,i,j} = \frac{\sum_{k=N_{g,lower}}^{N_{g,upper}} C_{k,i,j}}{\sum_{k=N_{g,lower}}^{N_{g,upper}} E_{k,i,j}} , \quad (6)$$

where

g = energy group number

k = index of the energy point within a group, where k ranges from $N_{g,lower}$ to $N_{g,upper}$

$C_{k,i,j}$ = MCNP calculation at the energy point k in energy group g, for scattering angle index i and sample thickness j

$E_{k,i,j}$ = experimental result at the energy point k in energy group g, for scattering angle index i and sample thickness j.

The sums used to calculate C/E are proportional to the areas under the calculated and experimental scattering spectra in a specified energy range. This area has physical meaning and is related to the scattering reaction rate over the specified energy range and angle. If the sum is carried out over the entire energy range, the result is referred to as the "total integrated C/E," or $(C/E)_{0,i,j}$.

The statistical error on the C/E value in each energy group g is

$$\Delta_{(C/E)_{g,i,j}} = \pm (C/E)_{g,i,j} \sqrt{\left(\frac{\Delta C}{C}\right)^2_{g,i,j} + \left(\frac{\Delta E}{E}\right)^2_{g,i,j}} , \quad (7)$$

where ΔC and ΔE are the statistical error in the MCNP calculation and the experimental data, respectively. The indices i and j are, once again, the angle number (index) and thickness number (index), respectively.

A C/E with a value of unity signifies a perfect match between MCNP calculation and experiment. The C/E values that deviate from unity signify a difference between the MCNP calculation and experiment. Differences between the experimental data and the MCNP calculations will give insight into the energy and angular regions where the nuclear data used for the calculations may need improvement.

A figure of merit (FOM) was calculated to assess which library has the best overall match to the experimental data (over all angles and thicknesses). The FOM is defined as a weighted deviation from unity [Eq. (8)] for each of the C/E columns in Table III:

$$\text{FOM} \equiv \frac{1}{N_\Omega} \frac{1}{N_t} \sum_{i=1}^{N_\Omega} \left[\sum_{j=1}^{N_t} \frac{[1 - (C/E)_{0,i,j}]^2}{\Delta^2_{(C/E)_{0,i,j}}} \right] , \quad (8)$$

where

$(C/E)_{0,i,j}$ = total integrated C/E value for detector angle index i and sample thickness index j

$\Delta_{(C/E)_{0,i,j}}$ = error (statistical plus systematic) for the total integrated C/E value for detector angle index i and sample thickness index j

N_Ω = total number of detector angles

N_t = total number of sample thicknesses.

The nuclear data library with the lowest FOM is considered to have the best overall match to the experimental data. It should be noted that the FOM cannot distinguish whether differences between the calculation and the experiment result from inaccuracies in the neutron scattering cross section or the underlying angular distribution used in the library.

VI. RESULTS AND DISCUSSION

Carbon was chosen as a reference since it has a cross section that was extensively measured and there is good agreement among all of the investigated nuclear data libraries. The carbon data were, therefore, used to validate that the scattering system was operating correctly during the experiment. Since carbon is a reference, there should be agreement between the MCNP calculations and the experimental data for the 7-cm-thick carbon sample. Any disagreement between the carbon MCNP calculations and experiment was interpreted as an inaccuracy in the detector system. Such inaccuracies were treated as systematic error in the results.

Figure 4 shows a comparison between calculation and experiment for the 7-cm-thick carbon sample at detector angles of 26, 72, 90, and 140 deg. Since all of the evaluated libraries agree for carbon, only ENDF-7.0 is shown in Fig. 4 for comparison. There is good agreement between experimental carbon and the corresponding MCNP calculation below 4 MeV and above ~9 MeV, thereby giving confidence that the experiment was performed correctly. The structure in the spectra below 2 MeV is attributed mostly to neutron transmission through air because carbon has little structure in this energy region. Structure above 2 MeV is dominated by carbon, most pronounced at the forward and backward angles.

There is some disagreement between the carbon experiment and the calculation in the energy range of 4 to ~9 MeV. At this point in time, it is uncertain what caused the disagreement in this energy region. Potential

TABLE III

Total Integrated *C/E* Values Between 0.5 and 20.0 MeV for All Samples and Detector Angles*

Angle (deg)	Sample	ENDF-7.0	ENDF-6.8	JEFF-3.1	JENDL-4.0
26	Zr 6 cm	1.010 (0.001) [0.02]	1.033 (0.001) [0.02]	1.050 (0.001) [0.02]	1.055 (0.001) [0.01]
	Zr 10 cm	0.946 (0.001) [0.02]	0.967 (0.001) [0.02]	0.989 (0.001) [0.02]	0.993 (0.001) [0.01]
52	Zr 6 cm	0.985 (0.001) [0.01]	0.971 (0.001) [0.01]	1.009 (0.001) [0.01]	1.010 (0.001) [0.01]
	Zr 10 cm	1.057 (0.001) [0.01]	1.042 (0.001) [0.01]	1.085 (0.001) [0.01]	1.084 (0.001) [0.01]
72	Zr 6 cm	1.055 (0.002) [0.01]	1.026 (0.002) [0.01]	1.044 (0.002) [0.01]	1.043 (0.002) [0.01]
	Zr 10 cm	1.056 (0.002) [0.01]	1.031 (0.002) [0.01]	1.050 (0.002) [0.01]	1.050 (0.002) [0.01]
90	Zr 6 cm	1.063 (0.001) [0.01]	1.042 (0.001) [0.01]	1.014 (0.001) [0.01]	1.014 (0.001) [0.01]
	Zr 10 cm	1.092 (0.001) [0.01]	1.074 (0.001) [0.01]	1.051 (0.001) [0.01]	1.048 (0.001) [0.01]
108	Zr 6 cm	1.047 (0.002) [0.01]	1.060 (0.002) [0.01]	0.971 (0.002) [0.01]	0.971 (0.002) [0.02]
	Zr 10 cm	1.053 (0.002) [0.01]	1.065 (0.002) [0.01]	0.985 (0.002) [0.01]	0.986 (0.002) [0.02]
120	Zr 6 cm	1.022 (0.002) [0.01]	1.061 (0.002) [0.01]	0.949 (0.002) [0.01]	0.950 (0.002) [0.02]
	Zr 10 cm	1.036 (0.001) [0.01]	1.076 (0.001) [0.01]	0.970 (0.001) [0.01]	0.969 (0.001) [0.03]
140	Zr 6 cm	0.969 (0.001) [0.01]	1.065 (0.002) [0.01]	0.958 (0.001) [0.01]	0.956 (0.001) [0.02]
	Zr 10 cm	0.970 (0.001) [0.01]	1.061 (0.001) [0.01]	0.955 (0.001) [0.01]	0.955 (0.001) [0.02]
154	Zr 6 cm	0.952 (0.002) [0.01]	1.093 (0.002) [0.01]	0.999 (0.002) [0.01]	1.000 (0.002) [0.02]
	Zr 10 cm	0.927 (0.002) [0.01]	1.056 (0.002) [0.01]	0.969 (0.002) [0.01]	0.968 (0.002) [0.02]
FOM		19 ± 2	23 ± 2	12 ± 2	10 ± 2

*Statistical error is shown in parentheses, and the systematic error is shown in square brackets. The figure of merit for each library is also presented.

causes of this disagreement may be one or more of the following: (a) the present treatment of efficiency of the detector system is not accurate in this region, (b) the photo-nuclear production cross-section library used to generate the MCNP incident flux shape is not accurate (e.g., ^{16}O), (c) the signal pulses from the detector PMTs were very large and distorted, and (d) the carbon data in the evaluation need improvement. The difference between the carbon measurement and the MCNP calculation was quantitatively treated as a systematic error in the final results. This systematic error also includes any error in the normalizations of the MCNP-calculated spectra to the experimental spectra. Ultimately, the disagreement between the carbon experiment and the calculation in the energy range of 4 to ~9 MeV results in relatively large statistical error in the *C/E* values for this energy group.

The zirconium experimental data and corresponding MCNP calculations for 6-cm and 10-cm thicknesses at detector angles of 26, 52, 72, 90, 108, 120, 140, and 154 deg are shown in Figs. 5 through 8. Visual differences were noticed between the experimental data and the MCNP calculations with different neutron cross-section libraries, especially at backward angles such as 154 deg. The differences noticed between ~4 and ~9 MeV were of the same magnitude as the differences in the carbon verification results presented in Fig. 4. Therefore, these differences were attributed to the systematic issue with the detector system rather than a real difference stemming from the nuclear cross-section libraries of zirconium.

A more quantitative approach to assess the significance of differences between the zirconium experimental data and the MCNP calculations is to explicitly calculate the *C/E* values. The *C/E* values are plotted for all detector angles in Figs. 9 and 10 for the 6-cm zirconium sample and in Figs. 11 and 12 for the 10-cm zirconium sample. The error bars in Figs. 9 through 12 are equal to the sum of the statistical error (1σ value) and the systematic error. This sum is defined as the uncertainty.

A total integrated *C/E* value was calculated that reflects the total area under the scattering spectrum and is shown in Table III. The statistical error (1σ value) is included in parentheses next to all values. The systematic error from the carbon measurement is included in square brackets.

The *C/E* values are interpreted based on the following characteristics:

1. When the *C/E* value differs from unity by more than the uncertainty (statistical plus systematic), the result is considered a significant difference.

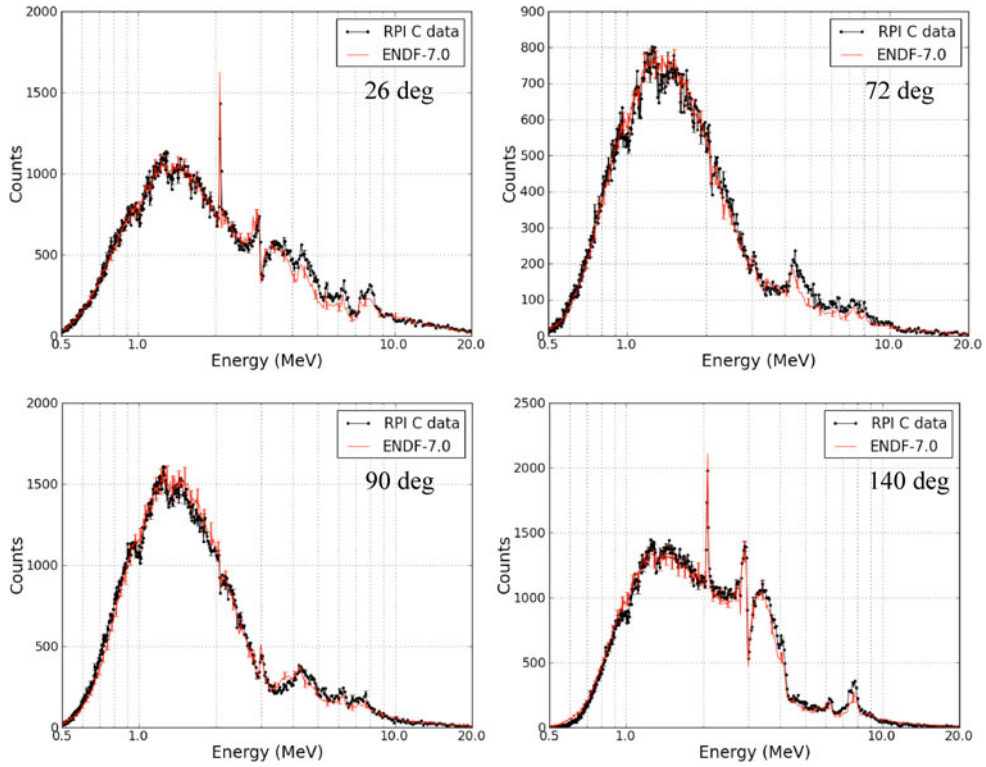

Fig. 4. Carbon (7.5-cm-diam × 7-cm-thick) neutron scattering measurements at 26, 72, 90, and 140 deg. The experimental carbon data are a result of PSA.

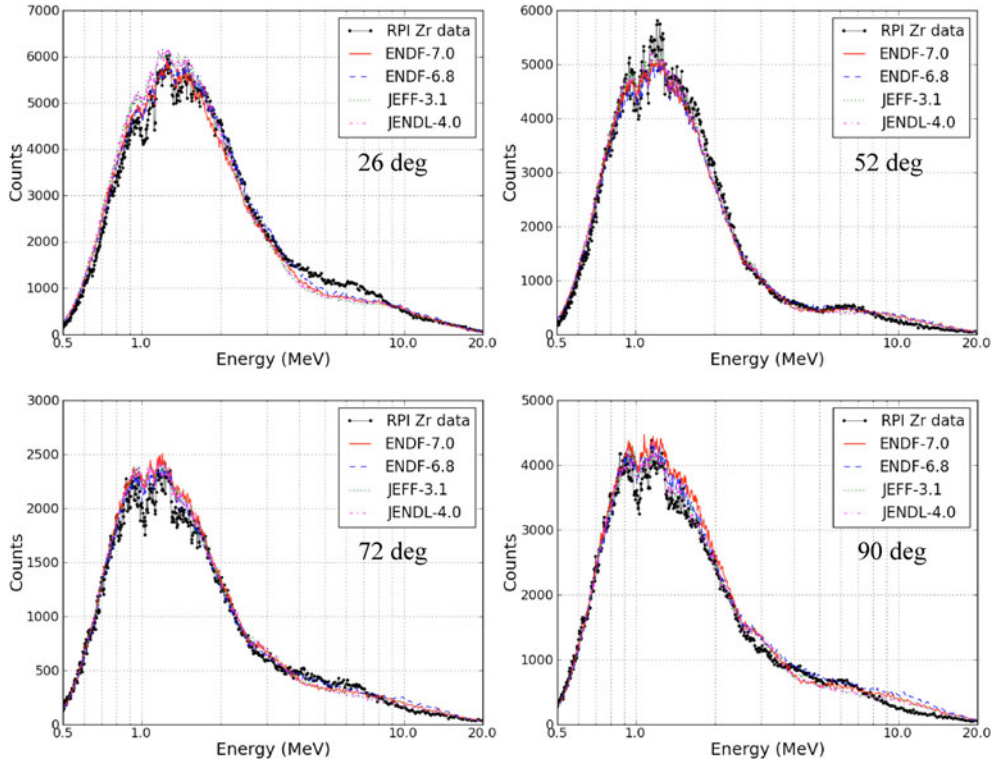

Fig. 5. Zirconium (7.62-cm-diam × 6-cm-thick) neutron scattering measurements at 26, 52, 72, and 90 deg. The experimental zirconium data are a result of PSA.

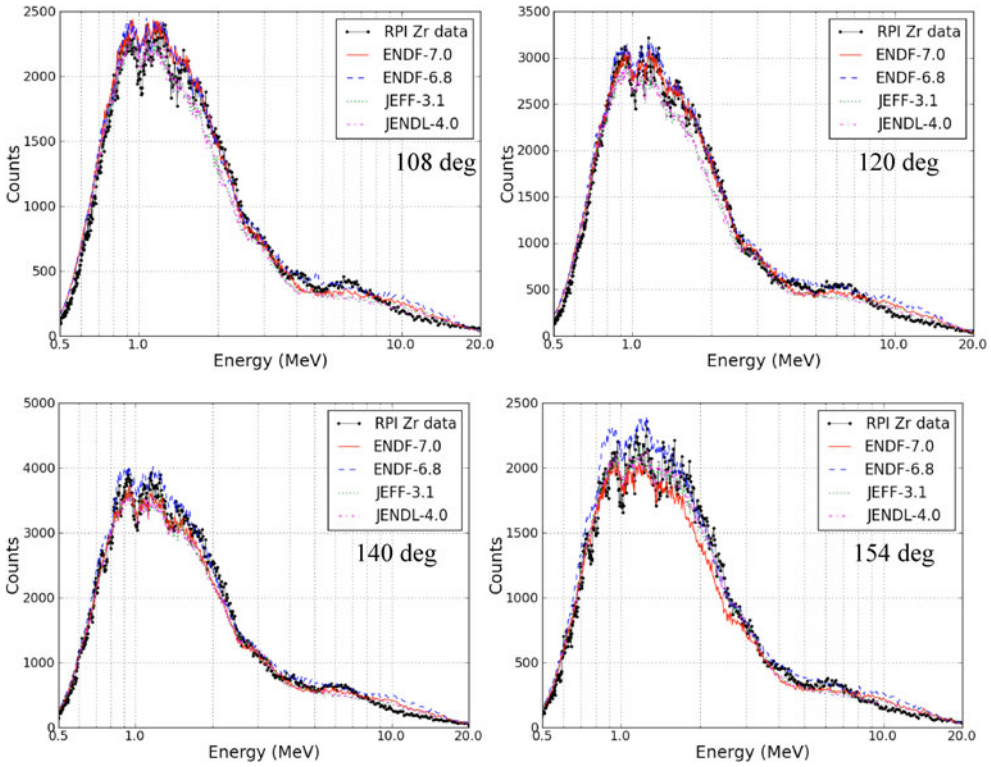

Fig. 6. Zirconium (7.62-cm-diam × 6-cm-thick) neutron scattering measurements at 108, 120, 140, and 154 deg. The experimental zirconium data are a result of PSA.

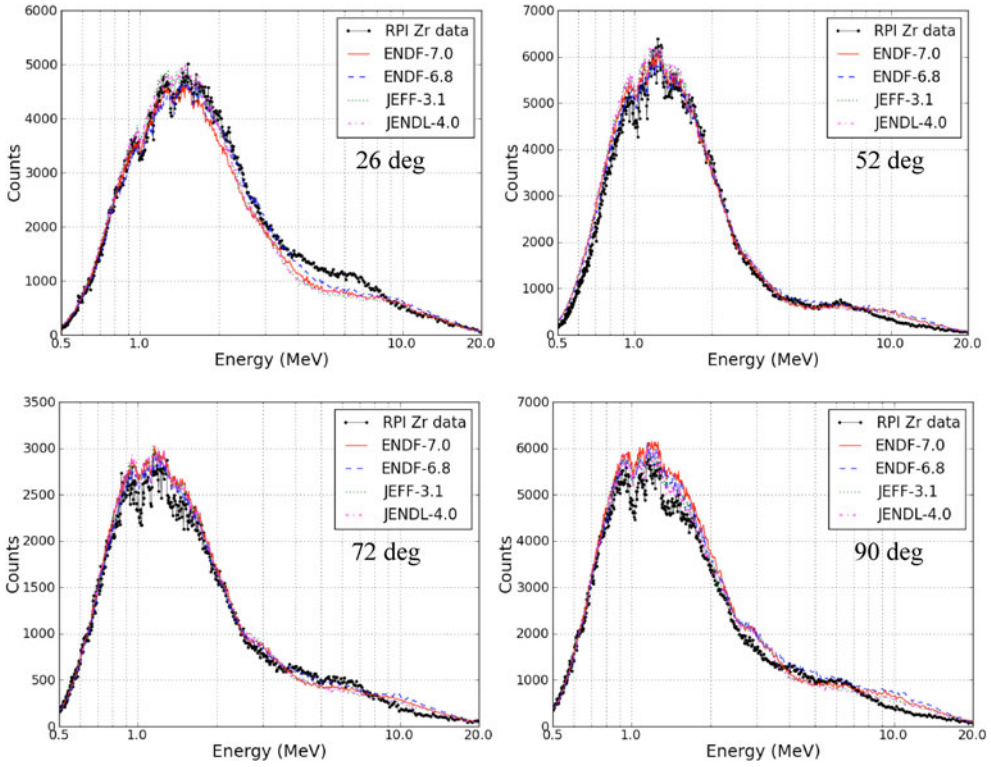

Fig. 7. Zirconium (7.62-cm-diam × 10-cm-thick) neutron scattering measurements at 26, 52, 72, and 90 deg. The experimental zirconium data are a result of PSA.

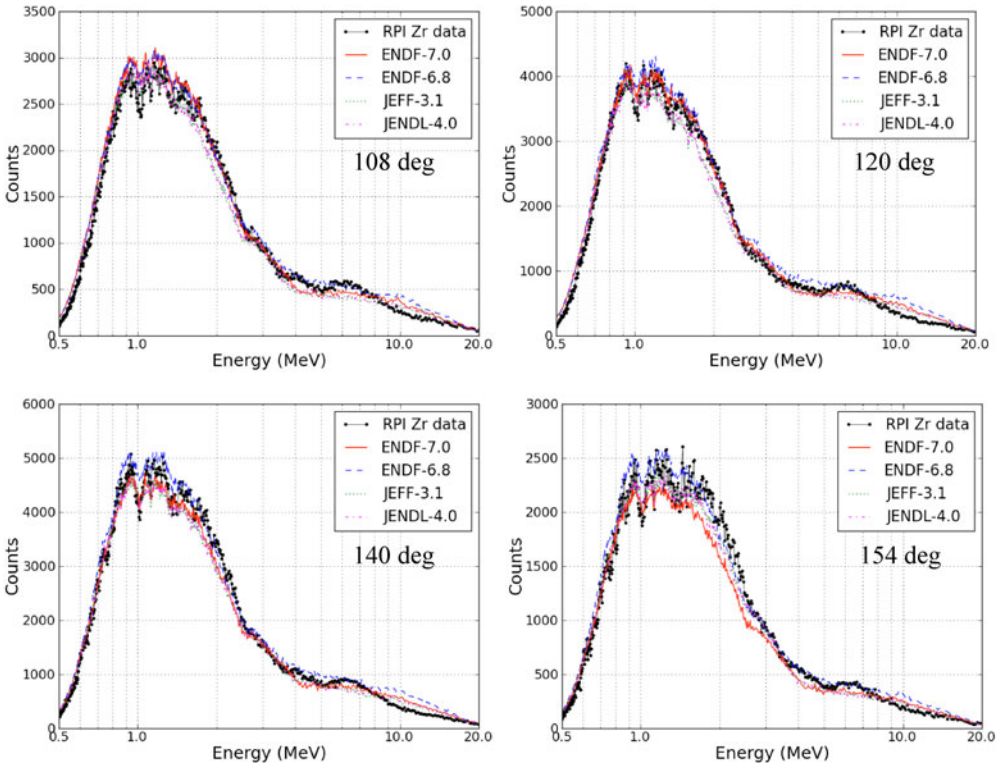

Fig. 8. Zirconium (7.62-cm-diam × 10-cm-thick) neutron scattering measurements at 108, 120, 140, and 154 deg. The experimental zirconium data are a result of PSA.

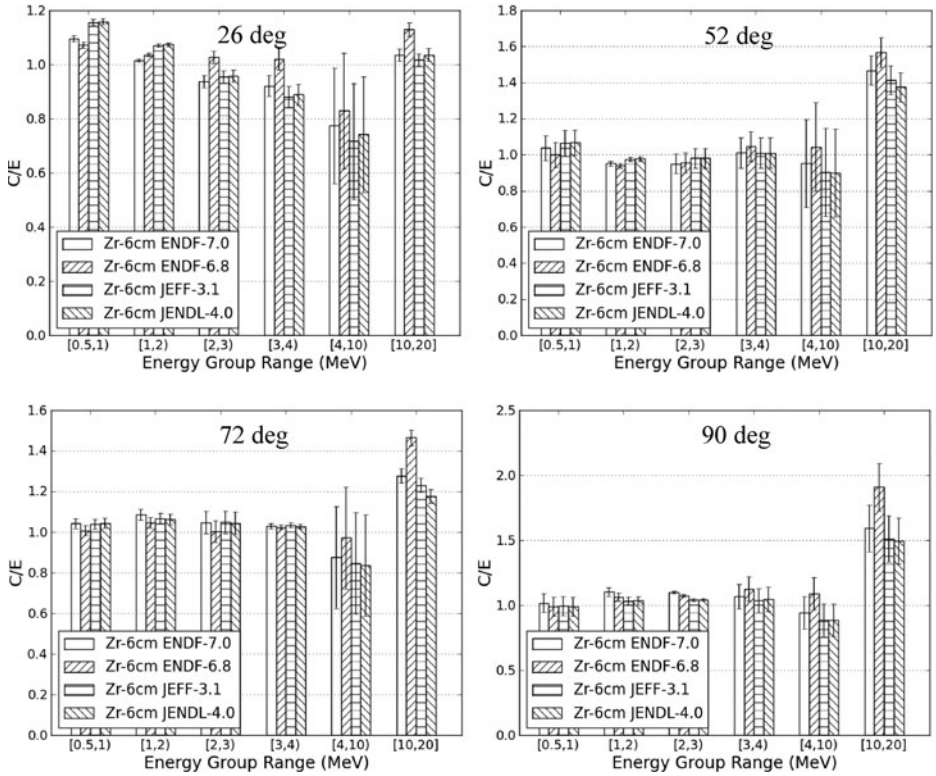

Fig. 9. *C/E* values for the 6-cm-thick zirconium sample at 26, 52, 72, and 90 deg. The error bars on these plots include both statistical and systematic error.

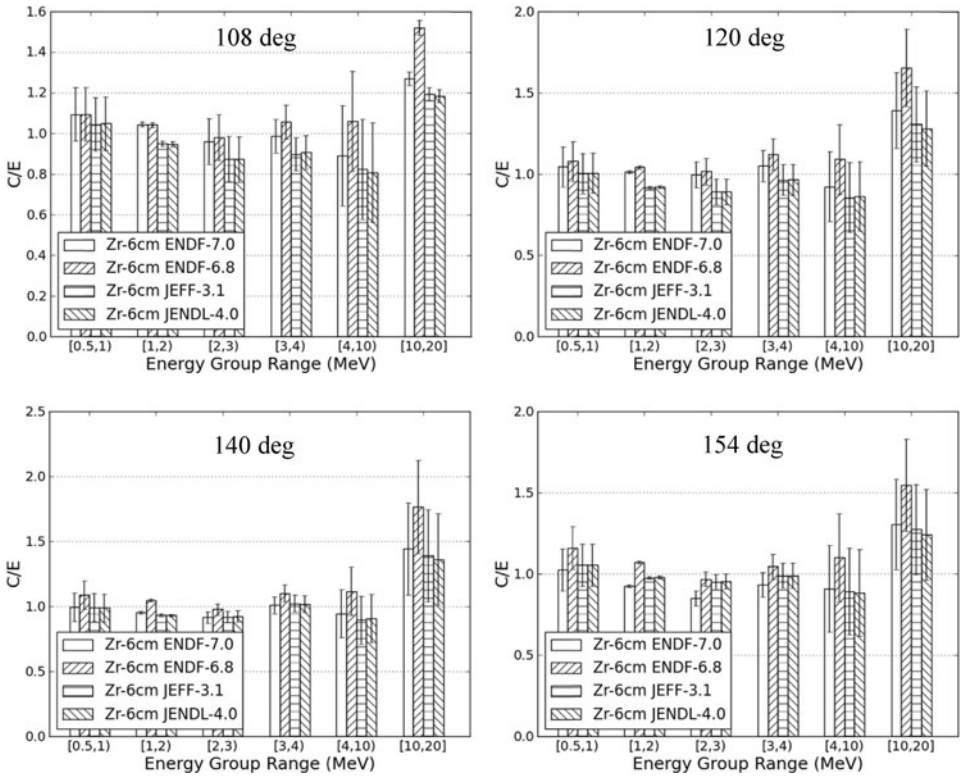

Fig. 10. *C/E* values for the 6-cm-thick zirconium sample at 108, 120, 140, and 154 deg. The error bars on these plots include both statistical and systematic error.

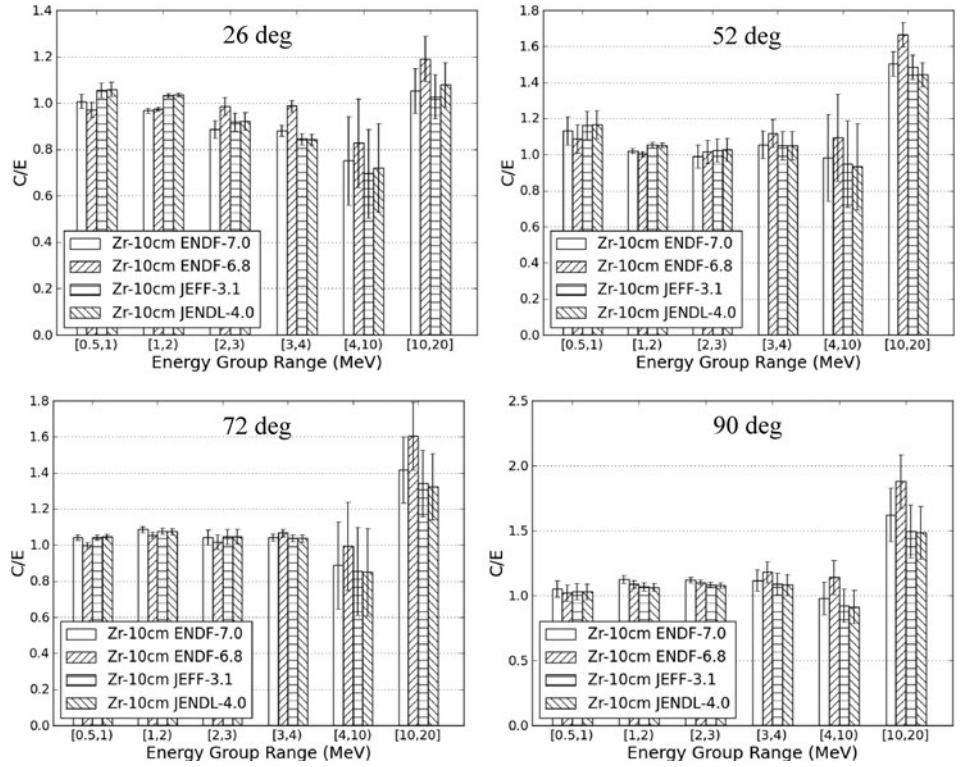

Fig. 11. *C/E* values for the 10-cm-thick zirconium sample at 26, 52, 72, and 90 deg. The error bars on these plots include both statistical and systematic error.

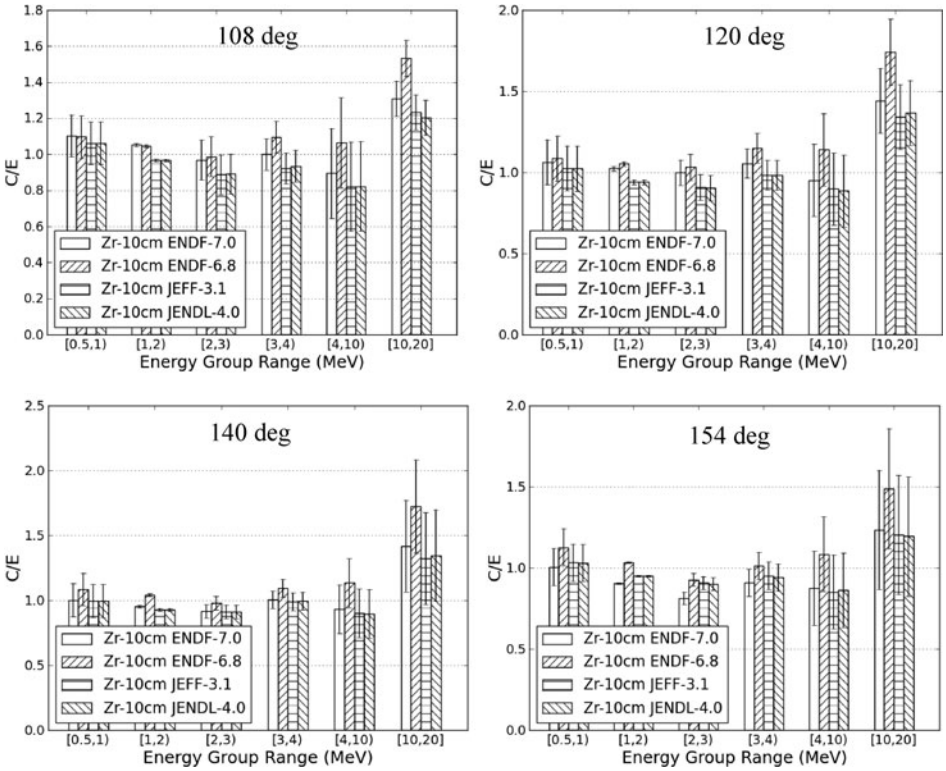

Fig. 12. *C/E* values for the 10-cm-thick zirconium sample at 108, 120, 140, and 154 deg. The error bars on these plots include both statistical and systematic error.

2. If the *C/E* values for both sample thicknesses agree and differ from unity (per above), then the conclusion is that the experimental data do not support the nuclear data library.

3. If the *C/E* values for both sample thicknesses disagree (for example, one being high and the other low), the result is inconclusive.

4. If the *C/E* value is greater than unity, then the experimental data are less than the calculated data. This implies that the scattering reaction rate is overpredicted in the calculation using that nuclear data library.

5. If the *C/E* value is less than unity, then the experimental data are greater than the calculated data. This implies that the scattering reaction rate is underpredicted in the calculation using that nuclear data library.

6. When the *C/E* value does not differ from unity by more than the uncertainty (statistical plus systematic) for both sample thicknesses, the calculation is said to match the data within the experimental uncertainty.

Inspection of Figs. 9 through 12 provided the following observations.

In the energy range from 0.5 to 1 MeV, the nuclear data libraries have *C/E* values equal to unity (within the error of the experiment) for a majority of the detector angles indicating that the libraries match the experimental data within error. All of the investigated nuclear libraries gave nearly the same number of matches to the experimental data and are considered equally good in this energy region. For the 6-cm sample at 26 deg and the 10-cm sample at 52 deg, the *C/E* values are significantly greater than unity (i.e., the interval of the $C/E \pm \Delta_{C/E}$ does not bound unity), ranging from approximately 1.05 to 1.2.

In the energy range between 1 and 2 MeV, a majority of the libraries had *C/E* values that significantly differed from unity. With the exception of ENDF-6.8 at 52 deg and 10 cm, the libraries did not match the experimental data for any of the detector angles. In this energy region ENDF-6.8 was higher than unity for all angles except 52 deg in the 6-cm sample. The JEFF-3.1 and JENDL-4.0 libraries were consistently lower than unity for angles >90 deg. All of the nuclear data libraries are about equally different from the experimental data.

Looking at the behaviors of both the 0.5- to 1.0-MeV group and the 2.0-MeV group provides some perspective. The error is larger for the 0.5- to 1-MeV group than for the 1- to 2-MeV group. Also, the *C/E* of a given library in the 0.5- to 1-MeV group appears to be well correlated to the *C/E* of that library in the 1- to 2-MeV group. Because both energy groups produce similar *C/E* values that are close to 1, but the lower energy group

produces larger error, naturally the lower energy group has more overlap, or agreement, with unity. This does not necessarily mean that the libraries are better in the 0.5- to 1-MeV group. Rather, it means that the experiment is better suited to perceive differences against the libraries in the 1- to 2-MeV group.

From 2 to 3 MeV, the ENDF-7.0 and ENDF-6.8 libraries matched a majority of the data. The JEFF-3.1 and JENDL-4.0 libraries had a majority of *C/E* values less than unity. The ENDF-7.0 and ENDF-6.8 libraries are comparable in this region, but ENDF-6.8 is slightly better.

In the energy region from 3 to 4 MeV, the ENDF-7.0, JEFF-3.0, and JENDL-4.0 libraries generally match the experimental data. The ENDF-7.0, JEFF-3.0, and JENDL-4.0 libraries all produce similar *C/E* values for this energy range. The ENDF-6.8 library had a majority of *C/E* values greater than unity for angles $\geq$72 deg.

In the energy range of 4 to 10 MeV, a majority of the libraries matched the experimental data within error. All libraries are comparable in this energy region. Agreement in this energy range is facilitated by the large uncertainties of these results. As discussed above, the relatively large error on the *C/E* values in this energy range is largely due to disagreements in the carbon reference experiment and calculations.

At high energies between 10 and 20 MeV, the majority of *C/E* values are greater than unity for all libraries. The JENDL-4.0 and JEFF-3.1 libraries match the data slightly better than ENDF-7.0. The ENDF-7.0, JEFF-3.0, and JENDL-4.0 libraries seem comparable. The ENDF-6.8 library has the highest *C/E* values for all angles and sample thicknesses.

The experimental data agree with all libraries within measured error in the following three regions:

1. $\geq$90 deg from 0.5 to 1 MeV
2. 52 deg from 2 to 3 MeV
3. 154 deg from 3 to 4 MeV.

The total energy integrated *C/E* values are shown in Table III. By inspection of the values, it can be seen that the maximum deviation between calculation and experiment was $\sim$9%. The values also indicate that for the forward angle of 72 deg and the side angle of 90 deg the libraries have *C/E* values greater than unity. At the backward angles of 108 and 120 deg, the ENDF-6.8 and ENDF-7.0 libraries have *C/E* values greater than unity while the JEFF-3.1 and JENDL-4.0 libraries have *C/E* values less than unity. The extreme backward detector angles of 140 and 154 deg show that the ENDF-6.8 library has *C/E* values greater than unity, while the ENDF-7.0, JEFF-3.1, and JENDL-4.0 libraries have almost all *C/E* values less than unity. The total integrated *C/E* values decrease with increasing sample thickness at the extreme forward and backward angles (26, 140, and 154 deg). However, the total integrated *C/E* values have the opposite sample thickness dependence at the other detector angles. The sample thickness effect on the *C/E* values may be due to complexities from multiple scattering.

A FOM was calculated that includes all detector angles and sample thicknesses for each nuclear data library. This FOM is included at the bottom of Table III and is representative of how each library matches the total scattering reaction rate. The FOM is also an indicator as to which library is the best match to the experiment overall. The JEFF-3.1 and JENDL-4.0 libraries have the lowest FOM values and agree with each other within error. Therefore, JEFF-3.1 and JENDL-4.0 are considered the libraries that best match the experimental data overall on this basis. It is noted that the FOM cannot distinguish whether differences between the calculation and the experiment result from inaccuracies in the neutron scattering cross section or the underlying angular distribution used in the library. Therefore, the FOM is useful for comparing libraries but is not sufficiently rigorous to answer the broader question of which library is "best."

VII. CONCLUSIONS

High-energy-neutron-scattering experiments for elemental zirconium were performed at the RPI LINAC in the energy region from 0.5 to 20 MeV. The experimental results were compared with MCNP calculations that simulated the experiment. The results show that the experimentally observed scattering cross section is significantly lower than all the evaluated libraries at energies between 10 and 20 MeV. For all energies and angles, the investigated nuclear data libraries agree with the experimental data to within 9%. This indicates that all investigated nuclear data libraries do a reasonable job overall. However, based on the overall FOM metric, JEFF-3.1 and JENDL-4.0 provide the best match to the experimental data.

ACKNOWLEDGMENTS

The authors would like to thank the RPI LINAC operators and staff: P. Brand, M. Gray, M. Strock, and A. Kerdoun, without whom these experiments could not have been performed.

REFERENCES

1. J. J. DUDERSTADT and L. J. HAMILTON, *Nuclear Reactor Analysis*, Wiley & Sons, New York (1976).

2. M. B. CHADWICK et al., "ENDF/B-VII.0: Next Generation Evaluated Nuclear Data Library for Nuclear Science and Technology," *Nucl. Data Sheets*, **107**, 2931 (2006).

3. A. KONING et al., "The JEFF-3.1 Nuclear Data Library," JEFF Report 21, Nuclear Energy Agency (2006).

4. K. SHIBATA et al., "JENDL 4.0: A New Library for Nuclear Science and Engineering," *J. Nucl. Sci. Technol*., **48**, 1 (2011).

5. A. B. SMITH and P. T. GUENTHER, "Fast-Neutron Scattering Cross Sections of Elemental Zirconium," ANL/NDM-69, Argonne National Laboratory (1982).

6. "MCNP—A General Monte Carlo Code for Neutron and Photon Transport, Version 5," LA-UR-05-8617, Los Alamos National Laboratory (2005).

7. M. E. OVERBERG et al., "Photoneutron Target Development for the RPI Linear Accelerator," *Nucl. Instrum. Methods Phys. Res., Sect. A*, **438**, 253 (1999).

8. F. SAGLIME, "High Energy Nuclear Differential Scattering Measurements for Beryllium and Molybdenum," PhD Thesis, Rensselaer Polytechnic Institute (2009).

9. F. J. SAGLIME et al., *Nucl. Instrum. Methods Phys. Res., Sect. A*, **620**, 401 (2010).

10. S. MARRONE et al., "Pulse Shape Analysis of Liquid Scintillators for Neutron Studies," *Nucl. Instrum. Methods Phys. Res., Sect. A*, **490**, 299 (2002).

11. R. BRUN and F. RADEMAKERS, "ROOT: An Object Oriented Data Analysis Framework": root.cern.ch/root (2004).

12. G. F. KNOLL, *Radiation Detection and Measurement*, Wiley & Sons, New York (2000).